

Pau Verdeguer Blom-Dahl

On the Interaction of High-Energy Gamma Radiation in the Active Galactic Nucleus of NGC 1068

A Theoretical and Computational Study.

Bachelor's Thesis

Supervisor: Michael Kacherließ

May 2025

Norwegian University of Science and Technology
Faculty of Natural Sciences
Department of Physics



Abstract

Active Galactic Nuclei (AGN) are some of the brightest objects in the universe, often outshining their entire host galaxy (Ghisellini, 2013). Comprehending the intricate structure and workings of these objects has driven decades of astronomical study. More recently, there has been growing interest in the role of high-energy neutrinos in these objects, as exemplified by the work of Eichmann et al. (2022). The IceCube collaboration (Abbasi et al., 2022) has detected a significant neutrino flux from the direction of NGC 1068, a Seyfert II galaxy located at a distance of approximately 10.1 Mpc. This has led to the conclusion that NGC 1068 is a source of high-energy neutrinos, produced alongside comparably energetic gamma rays. However, the observed gamma-ray luminosity in the GeV - TeV range is significantly lower than expected, as reported by the Fermi Gamma-ray Space Telescope in its 12-year survey (Abdollahi et al., 2022), prompting investigation into the cause of this discrepancy.

In this work, a model describing the propagation and reprocessing of high-energy gamma rays within the AGN, based on electromagnetic cascading, has been developed. For best-fit parameters, the model predicts a low-energy gamma-ray excess from reprocessed cascade photons in the $10^6 - 10^8$ eV range, which could be probed by future observations. The model also constrains the coronal radius to lie within 1 – 50 Schwarzschild radii, consistent with theoretical expectations.

Preface

The universe presents us with incredible extremes: temperatures, energies, and distances that defy everyday intuition. Perhaps most captivating among these are Active Galactic Nuclei, galactic cores housing supermassive black holes and emitting luminosities that can outshine their entire host galaxies. Initially, my interest in general astrophysics motivated me to seek a project in this research area. However, upon learning of the opportunity to work on these extreme objects, I became immediately interested. As I delved deeper into AGNs, I was struck by the complexity of their environments and the variety of phenomena they exhibit. The more I learned, the more I wanted to understand.

This project began with a simple but intriguing question: why would a galaxy like NGC 1068 be capable of producing high-energy neutrinos if not accompanied by the gamma-ray signal one would expect from the same pion decay? As I explored further into this anomaly, I discovered rich interaction between theory and observation, between what we see and what must be hidden. This led to the development of a model incorporating electromagnetic cascades to explain the attenuation of gamma rays while allowing high-energy neutrinos to escape.

As I wrote this work, I sensed the inspiration of the multi-messenger astronomy ethos—the idea that the universe is singing in many a voice, and that in listening to more than one, we better understand cosmic events. I hope that this research contributes modestly to the growing understanding of the high-energy cosmos and the powerful engines at galactic centers.

I am earnestly grateful to Dr. Kachelrieß, whose counsel and advice were invaluable for this work. Likewise, I also extend my gratitude to my family and friends, for their moral support and encouragement during the development of this project.

Contents

Abstract	i
Preface	ii
1 Introduction	2
1.1 Motivation	2
1.2 Objectives	3
2 Active Galactic Nuclei	4
2.1 Overview of AGNs	4
2.2 Radiation Mechanisms in AGNs	5
2.3 Gamma-ray and Neutrino Production in AGNs	8
2.4 Case Study: The AGN of NGC 1068	9
2.5 Neutrino Detection Techniques - IceCube	10
3 Modeling Approach	14
3.1 Theoretical Framework	14
3.2 Implementation	16
3.3 Simulation of Cascading via Random Walk	17
4 Results	20
4.1 Discussion	28
5 Outlook	29
5.1 Model Refinements	29
5.2 Computational Enhancements	30
5.3 Future Observational Tests	30
References	31

Chapter 1

Introduction

AGNs are among the most energetic and luminous objects in the universe. They are powered by the accretion of matter onto supermassive black holes at the centers of galaxies, leading to the emission of radiation across the entire electromagnetic spectrum (Ghisellini, 2013).

These objects have captured the interest of astronomers and astrophysicists for decades due to their complex nature. Understanding the physical processes that drive the emission of radiation from AGNs is essential for unraveling the mysteries of the universe and the fundamental laws of physics.

1.1 Motivation

In recent years, there has been a growing interest in the role that neutrinos play in high-energy astrophysical phenomena (Eichmann et al., 2022). Among these, AGNs have been identified as significant sources of high-energy particles, including gamma-rays and neutrinos.

One particular AGN, that of NGC 1068, has attracted attention due to its distinctive gamma-ray emission profile. Data from the IceCube collaboration (Abbasi et al., 2022) and Fermi-LAT (Abdollahi et al., 2022) indicate that, although the gamma-ray luminosity is expected to be comparable to the neutrino luminosity produced in the same region (Blanco et al., 2023), the observed gamma-ray luminosity in the GeV - TeV region is significantly lower than expected, as can be seen in Fig. 2.6.

The main mechanism why the observed gamma-ray flux is lower than one might naively expect from the neutrino flux (as seen by IceCube) can be expressed in the following manner:

- **Internal Absorption:** High-energy gamma rays produced within the corona interact with ambient photons via pair production ($\gamma\gamma \rightarrow e^+e^-$).
- **Electromagnetic Cascading:** These pairs initiate electromagnetic cascades, suffering energy losses via inverse Compton scattering off other background photons and synchrotron radiation, redistributing their energy to lower ranges.

This project's motivation arises from the aforementioned discrepancy between expected and observed fluxes of gamma rays coming from the AGN of NGC 1068. Developing a model to account for the interaction that these kinds of radiation suffer in

CHAPTER 1. INTRODUCTION

the AGN will be the main goal of this work. By simulating these interactions, I seek to deepen our comprehension of the high-energy phenomena in AGNs and contribute to the understanding of the mechanisms that govern the emission of gamma rays and neutrinos in these extreme environments.

1.2 Objectives

A series of goals have been defined to guide the research process throughout this project:

- Develop a physical model incorporating internal absorption and electromagnetic cascading to simulate the propagation of high-energy gamma rays through the AGN environment.
- Implement a realistic simulation of gamma-ray cascades in the AGN of NGC 1068, based on real physical phenomena, using a 3D Random Walk approach to simulate their interactions with the particles in the region.
- Compare the simulation results with observational data from the IceCube and Fermi-LAT collaborations to evaluate the model's accuracy and its consistency with the measured gamma-ray and neutrino spectra.

Chapter 2

Active Galactic Nuclei

2.1 Overview of AGNs

As technology improved throughout the 20th century, astronomers were able to observe the universe in different ways, discover new objects and phenomena that were unknown. Discoveries such as the cosmic microwave background and pulsars revolutionized our understanding of the universe and the laws of physics that apply to it.

The third major discovery, often mentioned alongside the cosmic microwave background and pulsars, is that of Active Galactic Nuclei, specifically quasars (“Quasi-stellar radio sources”), first introduced by Chiu (1964).

Active Galactic Nuclei are some of the most powerful and luminous objects in the universe and can outshine entire galaxies within a fantastically small volume. The energy output of these objects is so high that it is difficult to understand how they can produce it. The consensus is that this energy is produced by the accretion of matter onto a supermassive black hole, which typically has a mass ranging from 10^6 to 10^{10} M_\odot .

AGNs have diverse regions emitting different types of radiation. It is usually in the literature that we find the following components (Ghisellini, 2013):

- **The Supermassive Black Hole:** A black hole whose origin is still a source of speculation, but one which is believed to have emerged in the early universe. Its mass is $10^6 - 10^{10}$ solar masses, and is the source of the energy output in AGNs.
- **The Accretion Disk:** A ring-shaped mass of matter surrounding the black hole, slowly being accreted into it. Matter in the disk is heated to temperatures ranging from tens of thousands to millions of degrees, depending on a multitude of factors, such as the black hole’s mass and the region of the Disk. This heated matter produces radiation across the entire electromagnetic spectrum.
- **The Corona:** A region of hot, ionized gas located outside the accretion disk and believed to be the source of the X-ray emission in AGNs.
- **The Obscuring Torus:** A structure, likely toroidal or clumpy, composed of gas and dust that encircles the accretion disk and absorbs a portion of the radiation emitted, subsequently re-emitting it in the infrared region.

CHAPTER 2. ACTIVE GALACTIC NUCLEI

- **The Broad Line Region:** A region consisting of ionized gas formed by a number of small, fast-moving clouds in close proximity to the accretion disk. Doppler shifts broaden the observed lines, giving the region its characteristic name.
- **The Narrow Line Region:** Another region of ionized gas at a larger distance from the accretion disk, where less dense clouds are moving, less rapidly. The lower velocities of this region lead to narrower spectral lines.
- **The Jet:** About 10% of observed AGNs launch collimated jets of highly energetic particles, likely ejected from the poles of the black hole at relativistic velocities. Their appearance depends on the viewing angle. AGNs whose jets are pointing at us are called blazars. AGNs whose jets are pointing elsewhere are typically classified as radio galaxies.

Figure 2.1 illustrates the schematic structure of an AGN.

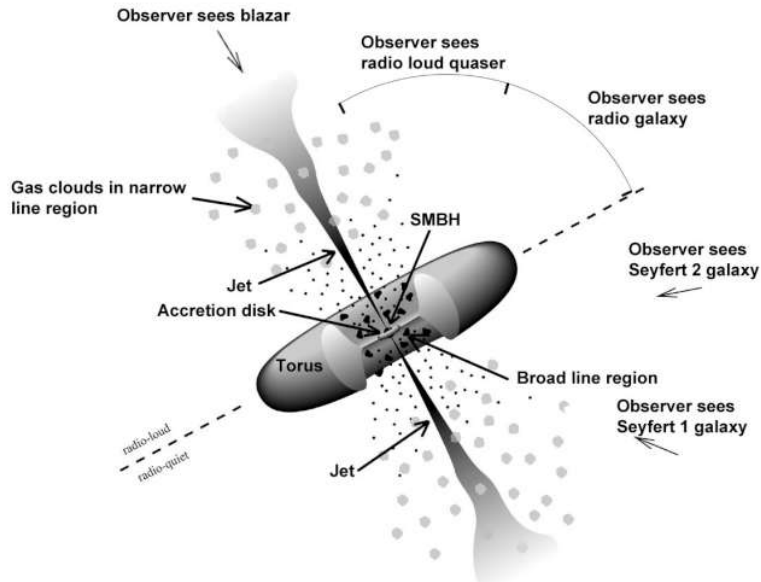


Figure 2.1: The general structure of an Active Galactic Nucleus. The different regions mentioned before are labeled. Figure taken from <https://fermi.gsfc.nasa.gov/science/eteu/agn/>

2.2 Radiation Mechanisms in AGNs

As stated, the main topic of this project is the production of gamma rays in the AGN of NGC 1068 and how they interact with the surrounding gas and radiation. We should first try to understand the underlying mechanisms that produce this type of radiation as well as all the types of radiation at play in such regions.

It is also essential to make a distinction between thermal and non-thermal emission processes. Thermal emission has its origin in hot matter in the AGN. It follows a

CHAPTER 2. ACTIVE GALACTIC NUCLEI

blackbody-like distribution, and is produced by particles which are in thermal equilibrium. Non-thermal emission, on the other hand, is produced by particles that are not in thermal equilibrium and are accelerated to high energies, thus producing radiation through different processes.

In general, AGNs emit the following types of radiation (Ghisellini, 2013):

- **Radio Emission:**

Synchrotron Radiation: It is generated by relativistic electrons moving in magnetic fields, which is common in AGN jets and lobes. In these sources, the spectrum typically covers photon energies from approximately 10^{-9} eV up to about 10^{-5} eV. In powerful radio-loud AGNs, this component can be extremely luminous, sometimes exceeding 10^{24} W Hz $^{-1}$.

Free-Free Emission: Generated by the interaction of free electrons with ions in the gas, which is common in HII regions (regions of ionized hydrogen).

Maser Emission: In some AGNs, molecules such as water in dense regions produce amplified microwave signals. This emission is typically observed around 10^{-6} eV and, while striking, generally represents only a minor fraction of the overall radio luminosity.

- **Infrared Emission:**

Thermal Dust Emission: Dust in the circumnuclear torus absorbs high-energy photons and re-emits them as energy in the infrared. The resulting spectrum spans energies from 0.001 to 1 eV. In obscured AGNs, this infrared component can dominate the bolometric output.

- **Optical/UV Emission:**

Thermal Emission: The inner parts of the accretion disk surrounding the supermassive black hole are heated to temperatures high enough to emit thermal radiation that peaks in the optical/UV band. This emission typically spans photon energies from about 1 eV to 10 eV, and in many unobscured AGNs it is the dominant contributor to the total luminosity.

Broad and Narrow Line Emission: In addition to the continuum, ionized gas in the broad-line and narrow-line regions produces characteristic spectral lines in the optical/UV. As an example, we have the H α line at 6563 Å (about 1.89 eV).

- **X-ray Emission:**

Non-thermal Emission: Relativistic electrons, primarily in the corona (up-scattering disk photons) and potentially in jets, produce X-rays via inverse Compton scattering, typically in the 0.1 keV to 100 keV range.

Bremsstrahlung: In certain AGNs, collisions in the hot gas produce thermal X-ray emission, which generally occurs over a similar energy interval (roughly 0.1 - 100 keV). Although significant, this process usually contributes less to the total X-ray luminosity than the non-thermal component.

- **Gamma-ray Emission:**

Inverse Compton Scattering: In the AGN's jets, high-energy electrons collide with low-energy background photons, boosting them to gamma-ray energies. This mechanism typically yields gamma rays in the range of 100 keV up to more than 10 GeV, and in some blazars, it forms a major part of the high-energy emission.

Proton-Proton Interactions: High-energy protons interacting with ambient protons can produce pions that decay into gamma rays (and neutrinos), often extending the spectrum into the TeV range (above 10^{12} eV).

Proton-Photon Interactions: Similarly, interactions between high-energy protons and low-energy photons lead to pion production and subsequent gamma-ray emission, further extending the high-energy tail into the TeV regime.

All in all, we get a complex distribution of energies in the AGN, with different processes producing different kinds of radiation. The overall resulting distribution of energies can be shown in what is known as a spectral energy distribution (SED) plot, which shows the luminosity of the AGN as a function of frequency. Figure 2.2 shows a schematic representation of the expected SED of a general AGN (excluding the radio and microwave bands, which are not shown).

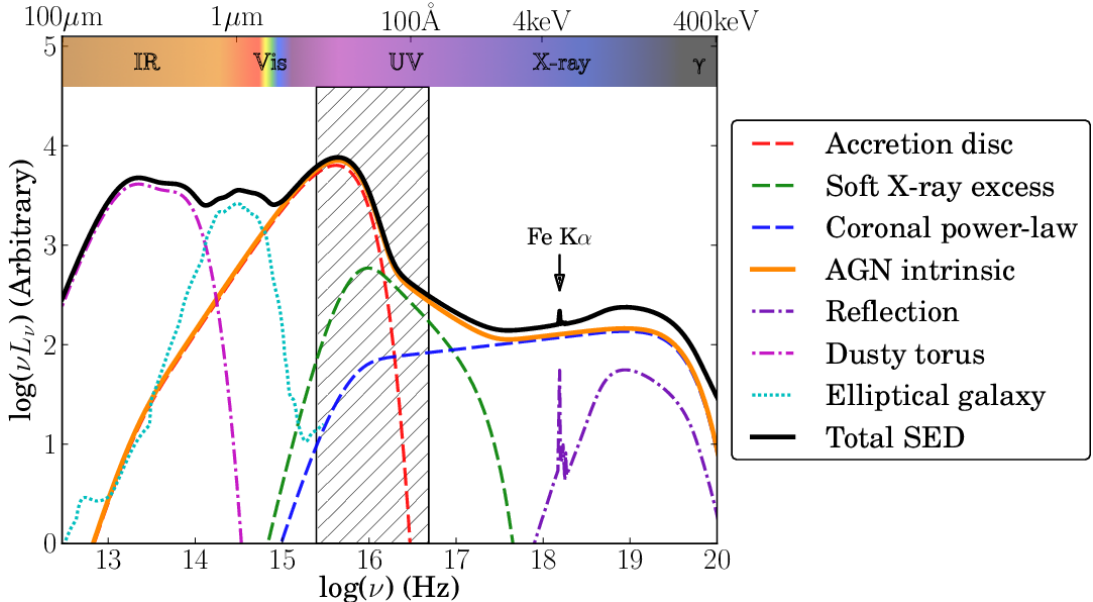


Figure 2.2: A simplified schematic diagram of an AGN SED, showing the approximate shape and extent of the various components discussed in the text. Dashed lines denote AGN intrinsic emission, dash-dot lines show emission reprocessed by the surrounding material, and the dotted line shows starlight from an elliptical host galaxy. The hatched region highlights a spectral range often subject to significant absorption by the Intergalactic medium (IGM). The example shows contributions from an elliptical host galaxy; galaxies with active star formation would exhibit stronger UV/IR components from stars and dust. Figure adapted from Collinson et al. (2016).

CHAPTER 2. ACTIVE GALACTIC NUCLEI

Proton-proton interactions and proton-photon interactions in the AGN of NGC 1068 are of special interest, since these processes also produce neutrinos, whose energy spectrum is related to the gamma-ray spectrum in a clear and predictable manner.

2.3 Gamma-ray and Neutrino Production in AGNs

We will focus on proton-proton and proton-photon interactions, which are sources of this type of radiation in AGNs.

Inside AGNs, close to the supermassive black hole, we find a region of hot, ionized gas, which is mainly composed of protons and electrons. These particles are accelerated to very high energies by mechanisms such as diffusive shock acceleration or magnetic reconnection (Padovani et al., 2024). The accelerated protons can then collide with other protons or photons in the gas, producing pions through the simplified processes specified below:

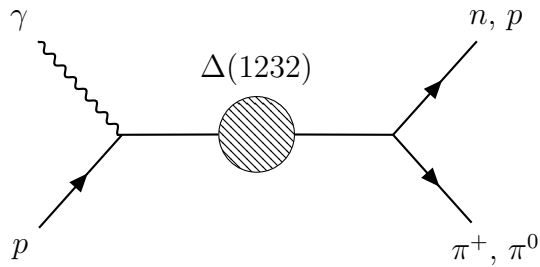


Figure 2.3: Simplified diagram for resonant proton-photon ($p\gamma$) interaction via the $\Delta(1232)$ resonance. Near resonance, the primary channels are $p\gamma \rightarrow \Delta^+ \rightarrow n\pi^+$ (approx. $2/3$ probability) and $p\gamma \rightarrow \Delta^+ \rightarrow p\pi^0$ (approx. $1/3$ probability).

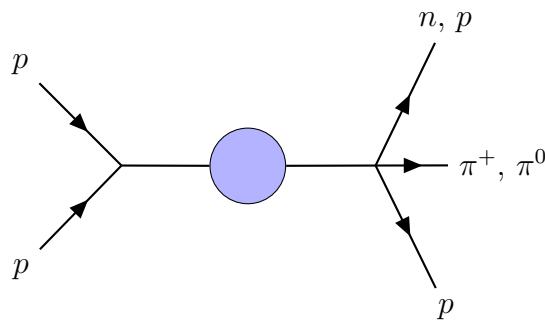
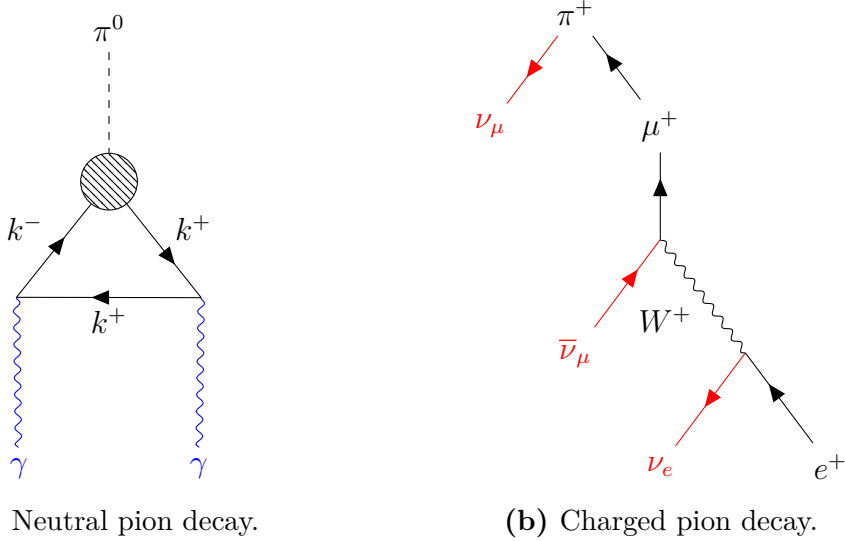


Figure 2.4: Simplified scheme for proton-proton interactions. The underlying interaction is represented by the blue circle.

The pions produced then decay into gamma rays and neutrinos through the following processes:



As highlighted in blue and red, the pions decay into gamma rays and neutrinos, respectively.

Crucially, since both gamma rays (from π^0 decay) and neutrinos (from π^\pm decay) originate from the same hadronic interactions, the neutrino flux detected from NGC 1068 implies an associated gamma-ray flux produced in the same source. The relationship between the fluxes is complex, but basic estimates suggest comparable energy outputs (Mücke et al., 1999). This is of great importance, since we can use the flux measured from the neutrinos as our initial estimate for the flux of gamma rays inside the AGN.

2.4 Case Study: The AGN of NGC 1068

NGC 1068 is a Seyfert type II galaxy located in the constellation Cetus, approximately 33 million light-years away from Earth¹. It is one of the closest AGNs to our galaxy, and has been the subject of numerous studies due to its unique properties. (Skrutskie et al., 2006)

The publication of neutrino data from the IceCube collaboration (Abbasi et al., 2022) has sparked numerous studies on the gamma-ray and neutrino emission from NGC 1068. Turning our attention to the SED of NGC 1068, we can see in Figure 2.6 that the gamma-ray emission, which should be comparable to the neutrino emission, is considerably lower.

In the figure, several features are highlighted:

1. The $\nu^{-0.7}$ radio spectrum.
2. A template for emission of the host galaxy.
3. A template for the accretion disk plus X-ray corona emission.

¹More on this value later (Padovani et al., 2024).

CHAPTER 2. ACTIVE GALACTIC NUCLEI

4. The γ -ray and neutrino bands.

Thus, the objective of this work will be to construct a model which can “shift” the energies from the neutrino spectrum to a distribution which is in agreement with the data points presented by Fermi-LAT and MAGIC.

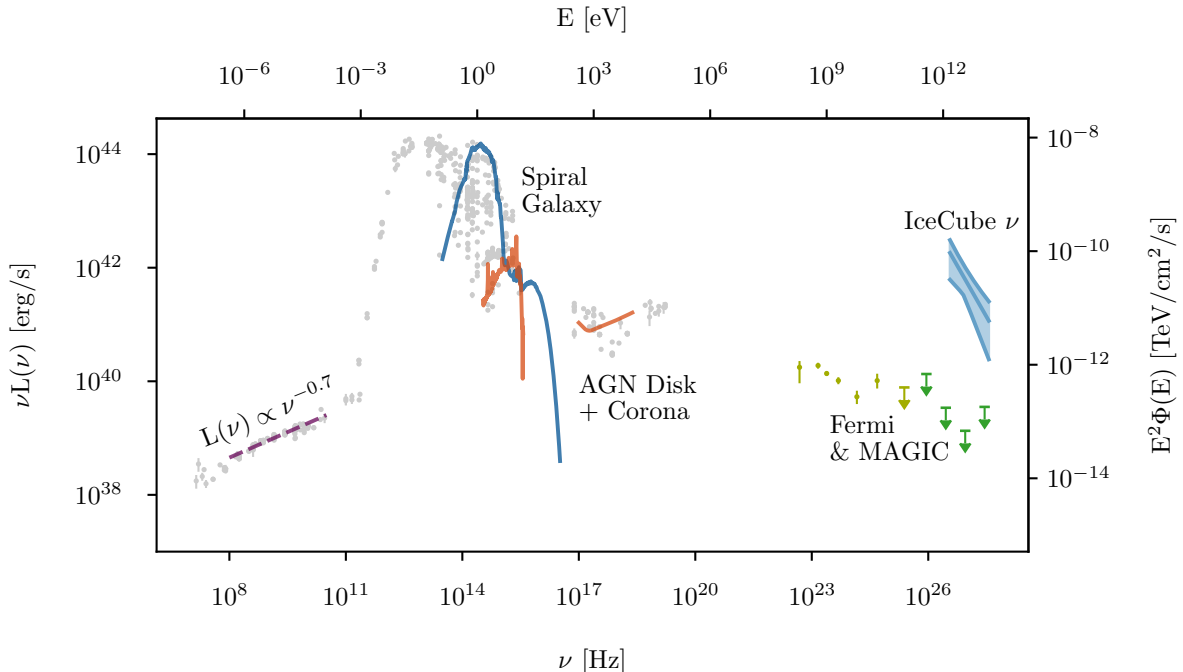


Figure 2.6: The integrated multi-messenger SED of NGC 1068, assembled using the SED builder at the SSDC (<https://tools.ssdc.asi.it/SED/>), showing the power emitted at different frequencies/energies; various components are highlighted. Note that the SED tool provides multiple values at the same frequency, which reflect the different resolutions used by the facilities which have studied the source on various spatial scales. For clarity we have kept mainly the highest flux values, which are associated with the largest scales, since the SED is dominated by the host galaxy given its relatively small distance. Figure taken from Padovani et al., 2024.

2.5 Neutrino Detection Techniques - IceCube

The process of detecting neutrinos is an essential part of this project, as data obtained from the IceCube Neutrino Observatory will be used as our initial flux estimate of gamma-rays inside the AGN’s corona.

The detection of neutrinos originating from distant astrophysical sources like NGC 1068 presents considerable experimental challenges due to their incredibly weak interaction with matter. This property, while making them near-perfect messengers of cosmic events, requires the construction of large-scale detectors in order to be able to detect them consistently.

CHAPTER 2. ACTIVE GALACTIC NUCLEI

The IceCube Neutrino Observatory, located at the geographic South Pole, represents the current state-of-the-art in high-energy neutrino detection (M.G. Aartsen et al., 2017). It utilizes a cubic kilometer of the deep, Antarctic glacial ice as both the target material and the detection medium. Embedded in the ice is an array of over 5,000 so-called Digital Optical Modules (DOMs): highly sensitive photodetectors encased in spherical glass pressure vessels. These DOMs are arranged on 86 vertical strings, deployed at depths between 1,450 and 2,450 meters. A schematic layout of the detector can be seen in Figure 2.7.

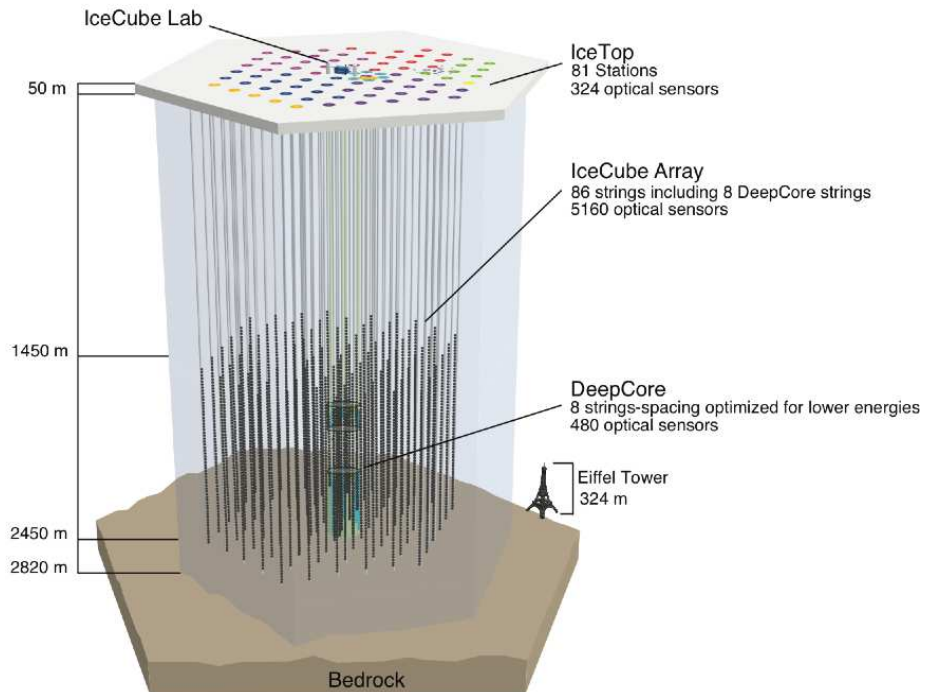


Figure 2.7: Schematic diagram illustrating the layout of the IceCube Neutrino Observatory beneath the Antarctic ice. The array consists of numerous vertical strings equipped with Digital Optical Modules (DOMs). Figure taken from M.G. Aartsen et al. (2017).

The detection principle which IceCube exploits relies on observing the Cherenkov radiation produced by secondary charged particles generated when a neutrino interacts within or near the instrumented ice volume. A high-energy neutrino (ν_l , where $l = e, \mu, \tau$) can interact with a nucleon (N) in an ice molecule via charged-current (CC) or neutral-current (NC) weak interactions:

- Charged Current (CC): $\nu_l + N \rightarrow l + X$
- Neutral Current (NC): $\nu_l + N \rightarrow \nu_l + X$

where l is the corresponding charged lepton (electron, muon, or tau) and X represents the resulting hadronic system.

CHAPTER 2. ACTIVE GALACTIC NUCLEI

If the charged secondary particles produced (the lepton l in CC interactions, or particles within the hadronic cascade X) travel through the ice faster than the speed of light in that medium (c/n , where $n \approx 1.31$ is the refractive index of ice), they emit Cherenkov radiation. This radiation manifests as a cone of faint blue light propagating through the ice, depicted conceptually in Figure 2.8. The DOMs detect the timing and intensity of this light.

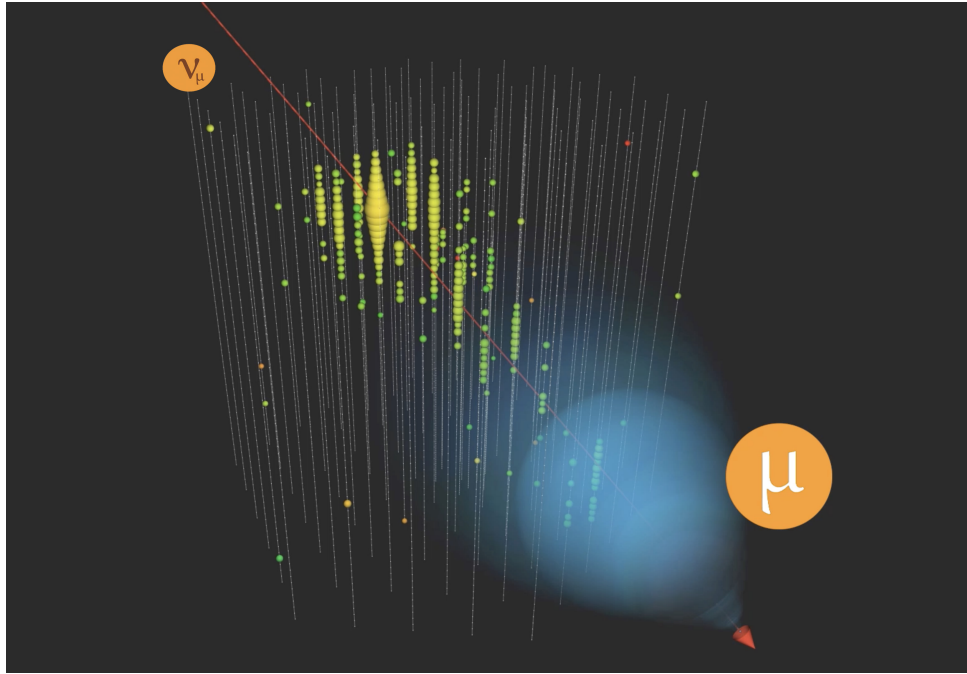


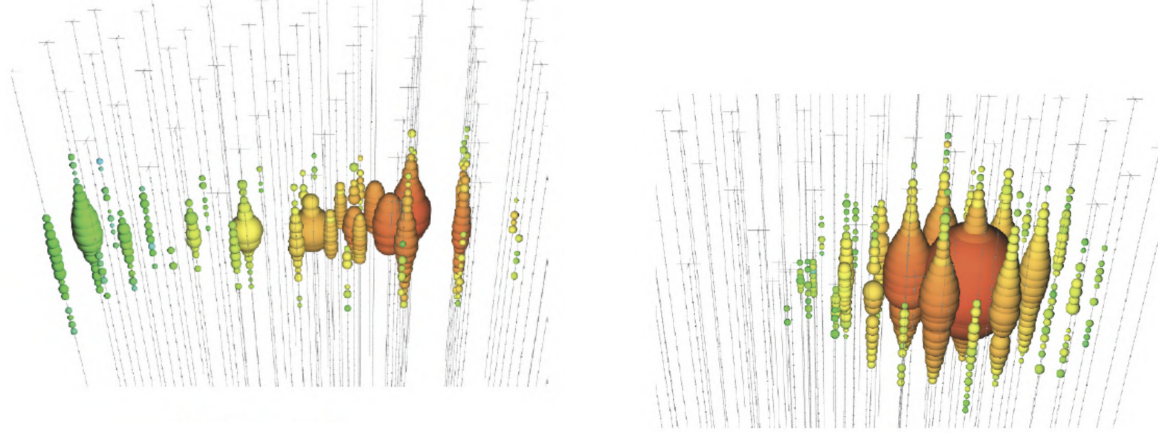
Figure 2.8: Conceptual illustration of Cherenkov radiation emitted by a muonic neutrino traveling faster than the speed of light in the ice medium. The light propagates in a cone, which is detected by the DOMs. Figure taken from <https://icecube.wisc.edu/gallery/measuring-the-neutrino-cross-section-with-earth-absorption/>

The shape of the detected light pattern allows for the classification of neutrino events and the reconstruction of their properties. Two primary event topologies are observed:

- **Tracks:** Primarily produced by muons generated in ν_μ CC interactions ($\nu_\mu + N \rightarrow \mu + X$). High-energy muons can travel several kilometers through the ice, producing long, linear tracks of Cherenkov light. The extended nature of these tracks allows for a relatively precise reconstruction of the muon's (and thus the incident neutrino's) direction, typically achieving sub-degree angular resolution for high-energy events. An example of a track event is shown in Figure 2.9a.
- **Cascades (or Showers):** Result from ν_e CC interactions ($\nu_e + N \rightarrow e^- + X$), ν_τ CC interactions ($\nu_\tau + N \rightarrow \tau + X$, where the tau lepton decays rapidly), and NC interactions of all neutrino flavors. In these events, the energy is deposited more locally, creating electromagnetic and/or hadronic showers. The resulting Cherenkov

CHAPTER 2. ACTIVE GALACTIC NUCLEI

light pattern is roughly spherical or elliptical and more contained. Cascades generally provide better energy resolution compared to tracks, as more of the initial neutrino energy is deposited within the detector volume, but offer poorer angular resolution (typically around $10^\circ - 15^\circ$). Figure 2.9b shows an example of a cascade.



(a) Example event display of a muon track signature in IceCube. The colored spheres represent DOMs, with color indicating arrival time and size indicating light intensity. The linear pattern allows for directional reconstruction.

(b) Example event display of a cascade signature in IceCube. The light is deposited more locally compared to a track, providing good energy information but poorer directional information.

Figure 2.9: Typical event topologies observed in the IceCube detector. Figures taken from Kowalski and IceCube Collaboration (2017)

By analyzing the spatio-temporal pattern of the light recorded by the DOMs, reconstruction algorithms determine the event's topology, estimate the neutrino's energy, and reconstruct its arrival direction. This directional data is essential for identifying potential astrophysical sources, such as the AGN of NGC 1068, by searching for statistically significant excesses of events clustered in specific regions of the sky above the large background of atmospheric neutrinos and muons. The detection of high-energy neutrinos coincident with known astrophysical objects offers strong proof for hadronic acceleration processes occurring within them.

Chapter 3

Modeling Approach

3.1 Theoretical Framework

We are interested in connecting the interaction rate per unit path length of a photon with energy E to the pair-production cross-section $\sigma_{\text{pair}}(s)$ and the spectral density of background photons $n_\gamma(\varepsilon)$. We can do so in the following manner (Kachelrieß et al., 2012)

$$R_\gamma(E) = \frac{1}{2} \int_0^\infty d\varepsilon n_\gamma(\varepsilon) \int_{-1}^1 d\mu (1 - \mu) \sigma_{\text{pair}}(s) \Theta(s - s_{\min}), \quad (3.1)$$

where s_{\min} is the threshold energy squared for pair production ($s_{\min} = 4m_e^2$ in this case, m_e being the mass of an electron), and $\Theta(s - s_{\min})$ is the Heaviside step function. It is there to ensure we only integrate over energies above the threshold. The pair-production cross-section $\sigma_{\text{pair}}(s)$ is well-known, as one can find in any particle physics textbook. It is given by

$$\sigma_{\text{pair}}(s) = \frac{3}{4} \sigma_{\text{Th}} \frac{m_e^2}{s} \left[(3 - \beta^4) \ln \frac{1 + \beta}{1 - \beta} - 2\beta(2 - \beta^2) \right], \quad (3.2)$$

where σ_{Th} is the Thomson cross-section, $\beta \equiv \sqrt{1 - 4m_e^2/s}$, $s = 2E\varepsilon(1 - \mu)$ and $\mu \equiv \cos(\theta)$, where θ is the angle between the incident high-energy photon (E) and the background photon (ε).

From equation (3.1), it is convenient to rewrite the integrals in terms of the mandelstam variable s , and swap the order of integration. Doing so, we get the following:

$$\begin{aligned} R_\gamma(E) &= \frac{1}{8E^2} \int_0^\infty \frac{d\varepsilon}{\varepsilon^2} n_\gamma(\varepsilon) \int_{s_{\min}}^{4E\varepsilon} ds s \sigma_{\text{pair}}(s) = \\ &= \frac{1}{8E^2} \int_{4m_e c^2}^{4E\varepsilon_{\max}} ds s \sigma_{\text{pair}}(s) \int_{\frac{s}{4E}}^{\varepsilon_{\max}} \frac{d\varepsilon}{\varepsilon^2} n_\gamma(\varepsilon) \end{aligned} \quad (3.3)$$

Notice that for a given s , we have $s \leq 4E\varepsilon$, which implies that $\varepsilon \geq \frac{s}{4E}$. This is the reason for the lower limit of the ε integral. The upper limit of the ε integral is ε_{\max} , which is the maximum energy of our background photons.

In order to find this interaction rate of photons with energy E , we need to know the spectral density of background photons $n_\gamma(\varepsilon)$. To derive this quantity, we first need to know what the spectral energy distribution of background photons looks like. Eichmann

CHAPTER 3. MODELING APPROACH

et al. (2022) derived in their work a spectrum of background photons for the starburst and X-ray corona region. This background spectrum will be used to model the density of background photons $n_\gamma(\varepsilon)$ inside the AGN's corona:

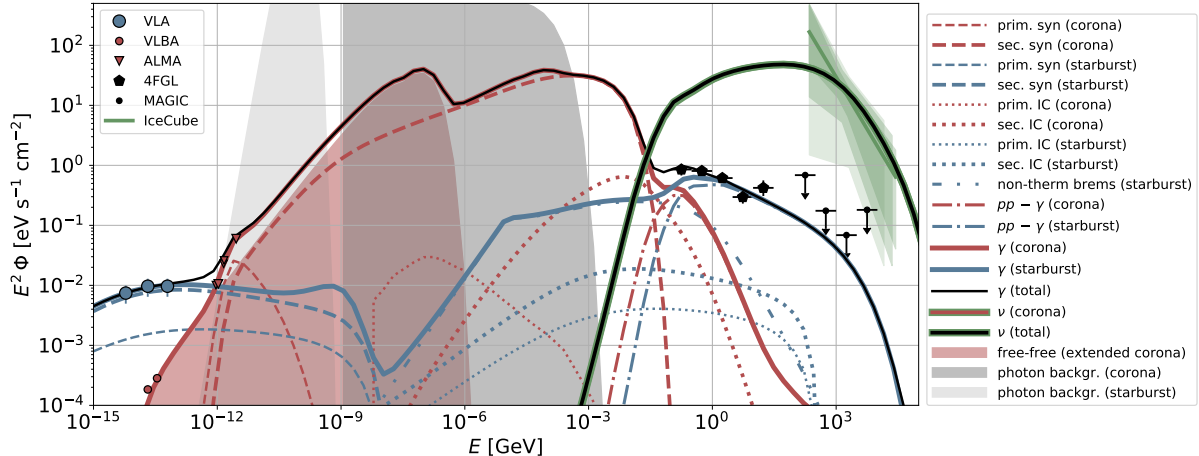


Figure 3.1: The model predictions of the *photon and neutrino* SED of NGC 1068 with respect to the data—red markers refer to a beam size of $\sim (0.02 - 0.06)$ arcsec, and black or blue markers indicate a beam size of $\gtrsim 10$ arcsec. The light red area shows the free-free emission from the extended corona. The dark grey area indicates the *internal* flux of the background (target) photon fields (disk- and torus emission as well as Comptonized X-rays of the AGN's corona) of the central AGN and the light grey area indicates the thermal IR emission by dust grains of the starburst region. Note that the torus attenuation is not taken into account here. Figure taken from Eichmann et al. (2022).

The red line marked as γ (corona) in the legend of the figure above will be used to model the spectral density of background photons $n_\gamma(\varepsilon)$ ¹.

$n_\gamma(\varepsilon)$ can be connected to $\Phi(\varepsilon)$ in the following manner: we know that the differential flux of background photons relates to the specific intensity $I(\varepsilon)$ by

$$\Phi = \int d\Omega I \cos \vartheta. \quad (3.4)$$

For a spherical source of radius R at a distance d , $\Omega = \pi \left(\frac{R}{d} \right)^2$

We can also connect $I(\varepsilon)$ to the spectral density of background photons $n_\gamma(\varepsilon)$ using

$$n_\gamma(\varepsilon) = \frac{4\pi}{c} I(\varepsilon), \quad (3.5)$$

where c is the speed of light. By combining equations (3.4) and (3.5), we can find the

¹It is important to note the circular reasoning here. Ideally, the cascaded spectrum should be used to simulate the cascading of the same particles. However, for simplicity, I will assume the aforementioned to be the pre-existing spectrum within the corona.

CHAPTER 3. MODELING APPROACH

spectral density of background photons $n_\gamma(\varepsilon)$ in terms of $\Phi(\varepsilon)$

$$n_\gamma(\varepsilon) = \frac{4}{c} \left(\frac{d}{R_c} \right)^2 \Phi(\varepsilon), \quad (3.6)$$

where d is the distance to the AGN, and R_c is the radius of the corona.

For this work, the distance to NGC1068 is assumed to be $d = 10.1$ Mpc. This value comes from Padovani et al. (2024). The coronal radius can be parametrized as $R_c = \eta R_s$, with $\eta \sim 10 - 100$, and R_s being the Schwarzschild radius of the black hole, calculated² to be around 1.4×10^{-6} pc.

A useful quantity to calculate is the optical depth of the corona. This relates to the probability of a photon with a certain energy interacting through pair production. The optical depth $\tau_{\gamma\gamma}$ is given by

$$\tau_{\gamma\gamma} = R_\gamma \cdot R_c.$$

Figure 3.2 shows the optical depth of the corona as a function of the energy of the photons for different values of R_c .

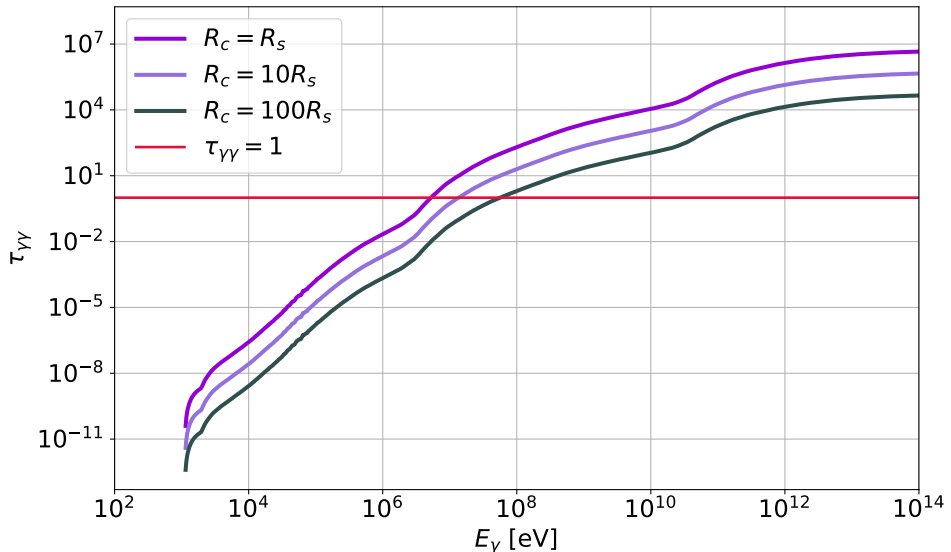


Figure 3.2: Optical depth of NGC1068's corona as a function of the energy of the photons, represented for different values of the corona radius. One can see that the corona is optically thick for high-energy photons ($\tau_{\gamma\gamma} > 1$), and optically thin for low-energy photons ($\tau_{\gamma\gamma} < 1$), meaning that high-energy photons are prone to interacting with the corona more than low-energy ones.

3.2 Implementation

The implementation of this model was performed in MATLAB. The code is available in Appendix A, and it is structured in the following way:

²Assuming a non-rotating Schwarzschild black hole with mass $M = 1.3 \times 10^7 M_\odot$ (Wang et al., 2020)

CHAPTER 3. MODELING APPROACH

- Initialization: Defines physical constants and loads observational data (e.g., from Fermi-LAT, IceCube) used for comparison. However, as we want to test the model for different values of certain parameters, these don't get defined here.
- Parameter Loops: Nested loops iterate over the model parameters being tested, such as the coronal radius (R_c), the initial radial distribution parameter (α , see Eq. 3.8), and the maximum turning angle (θ_{\max}).
- Interaction Rate Calculation: within the loops, the code calculates the interaction rate per unit length, $R_\gamma(E)$, using the theoretical framework (Section 3.1) for the current value of R_c . These values are stored in a matrix, as a function of the energy of the photons.
- Cascade simulation: Finally, the code calculates the cascading of photons in the corona, and stores the results for the parameters defined. It is assumed that the photons produced in the corona have the same energy distribution as that of the neutrinos we receive. This part is very intricate, and has different steps to it, which are detailed in Section 3.3.

3.3 Simulation of Cascading via Random Walk

There are several parameters which affect the cascading of photons in the corona. These include the coronal radius, the maximum turning angle of the particles and the alpha value, which controls the initial distribution of photons. The random walk is a stochastic process, and as such, it is important to consider the different sources of error one can encounter when developing these kinds of models, such as the number of particles simulated or the binning of the energy spectrum. The code is structured in a way that allows for easy modification of these parameters, so that one can test different values and see how they affect the results.

For each energy bin, a number of particles which is proportional to the flux at said energy is chosen to simulate. The particles are chosen according to the formula

$$\#_{\text{part.}, E} = \left\lfloor \rho \frac{\Phi_E \Delta_E}{\min(\Phi_E \Delta_E)} \right\rfloor, \quad (3.7)$$

Φ_E and Δ_E being the flux and bin width as a function of the energy. The latter of the two can be increased to reduce statistical noise. The numerator is divided by its minimum to ensure normalization: this way we make sure we simulate at the very least one particle for the lowest flux. Finally, ρ is a multiplicative factor, which can be changed to modify the overall number of particles we want to simulate. The program then rounds the resulting value to the nearest integer, giving the number of particles for each energy bin.

For each particle:

1. The initial position is randomly placed inside the corona using a power law of the shape

$$r = R_c \cdot \text{rand}^{(1/\alpha)}. \quad (3.8)$$

CHAPTER 3. MODELING APPROACH

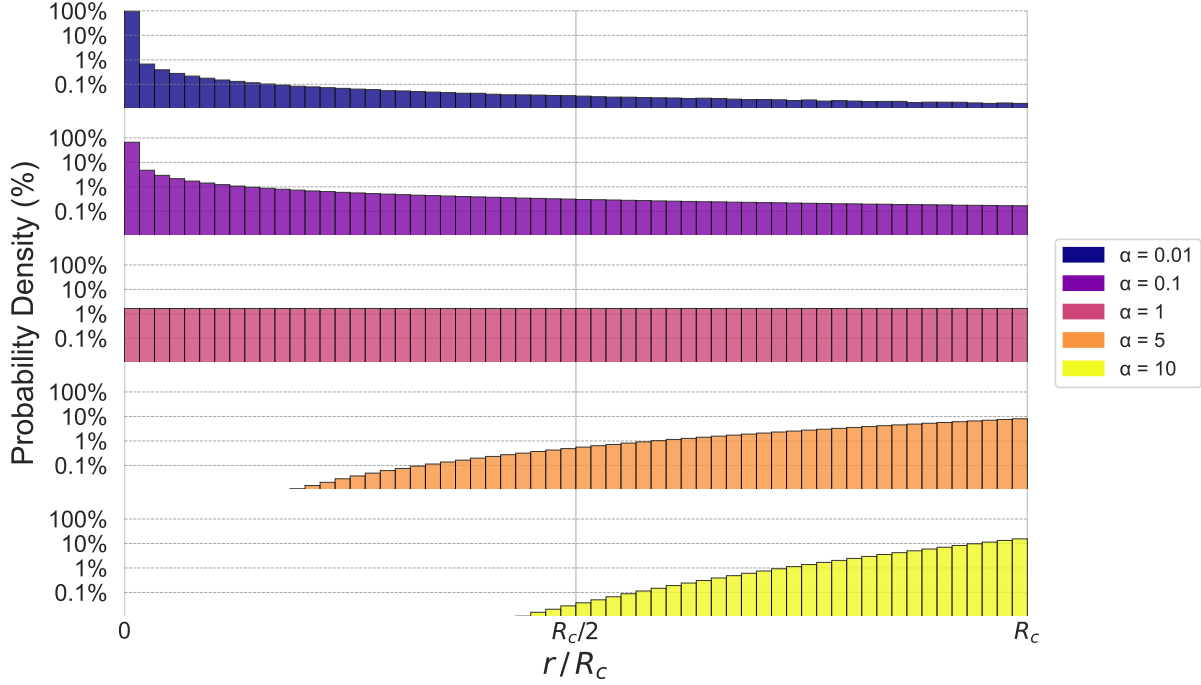


Figure 3.3: Initial distributions of the photons for different values of α . The y-axis shows the percentage of photons, and the x-axis shows the distance from the center of the corona. In order to account for the division by zero in the case of $\alpha = 0$, the program assumes all particles start at the origin in this case.

2. Each particle is assigned a random initial direction, uniformly distributed on a sphere.
3. The particle propagates until it exits the corona. Each step it takes has a length determined by

$$L = -\frac{\ln(\text{rand})}{R}, \quad (3.9)$$

where R is the interaction rate previously calculated as a function of the energy of the photon.

4. After each collision, the particle's direction is updated. The new direction is determined by a random angle θ sampled from a uniform distribution between $-\theta_{\max}$ and θ_{\max} .

³This is a simplification of the actual process. In reality, in order to achieve truly random directions (not biased towards the poles), the program generates uniformly distributed points on a spherical cap of max angle θ_{\max} around the z axis, which is then rotated to the previous direction. The random point selected becomes the new direction of the particle. The Manim folder inside the GitHub repository contains a visualization of this process.

CHAPTER 3. MODELING APPROACH

5. The particle's energy is multiplied by a random fraction sampled from a predefined probability distribution⁴. The probability distribution is defined in the code, and can be changed to test different distributions. The default one is a Gaussian distribution with a mean of 0.5 and a standard deviation of 0.01. This essentially means that the energy of the particle is multiplied by a random value between 0.49 and 0.51.⁵
6. In order to account for the energy lost in the process, which is transferred to the background photons, the program assumes that in every step a new particle is created with the exact same energy as the original photon, which cascades in the same way. Meaning we end up with 2^N particles with the same energy, N being the number of collisions in the cascade⁶.
7. Finally, in order to determine the flux as a function of the energy (proportional to the number of particles), the particles are binned logarithmically with spacing which is also specified in the program (Δ_E), and can be changed to reduce statistical noise, in turn reducing the need for computing a high number of particles.

⁴It must be noted that the process being modeled here omits the production of e^+e^- pairs, assuming they recombine quickly into gamma rays. Hence, the true physical process being modeled here is scattering of gamma rays, and not cascading.

⁵Here, another simplification is made. When two photons produce a pair and $E\varepsilon/m_e^2c^4 \gg 1$, the fraction of energy lost is $f \approx [\ln(2E\varepsilon/m_e^2c^4)]^{-1}$. However, if $E\varepsilon/m_e^2c^4 \sim 1$, $f = 0.5$. Thus, it is assumed that $\varepsilon \sim m_e^2c^4/E$. (Berezinsky and Kalashev, 2016)

⁶This is another approximation. In reality, one should consider the full cascade of each newly produced particle individually. However, this would increase computational costs exponentially.

Chapter 4

Results

Below is the path followed by a randomly selected particle with initial energy $E = 10^{14}\text{eV}$:

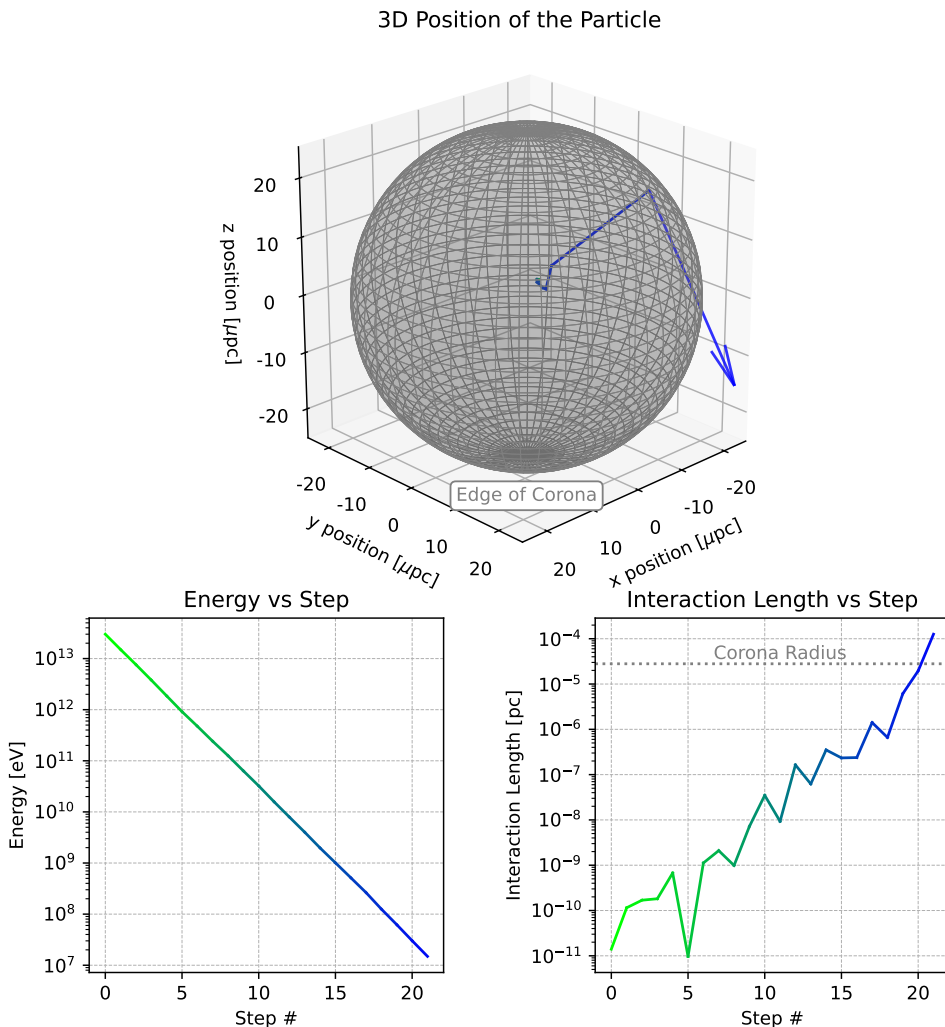


Figure 4.1: Magnitudes of the 3D random walk of a random particle ($\theta_{\max} = \pi, \alpha = 0$). The blue arrow indicates the last position is located outside the graph in said direction. Also represented are the energy of the particle in each step and the interaction length of every step. When this last one becomes bigger than R_c , the particle inevitably escapes.

CHAPTER 4. RESULTS

The energy of the particle gets reduced exponentially in every collision (a straight line in logarithmic representation). The final energy is expected to be close to $E_{\text{final}} = E_{\text{initial}} \cdot 0.5^{N_{\text{int}}}$, N_{int} being the number of interactions. Now, after binning the particles logarithmically according to their energy, we can build the simulated SED. The following plot shows the SED of NGC 1068's AGN for example values of the coronal radius, alpha and the maximum turning angle:

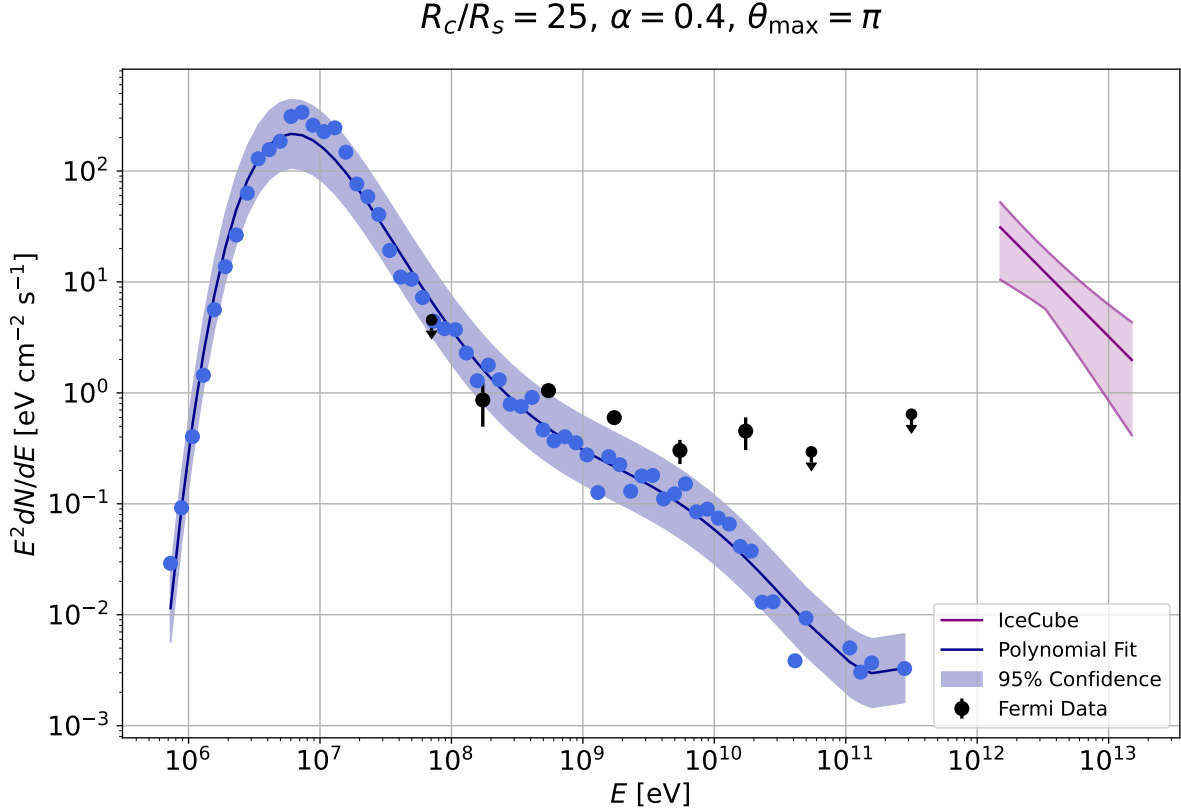


Figure 4.2: Spectral Energy Distribution of NGC 1068's AGN for $R_c = 25R_s$, $\alpha = 0.4$ and $\theta_{\max} = \pi$. The purple line represents the 10-year data from IceCube, as well as our initial flux for the photons. The blue dots are the simulated flux from the model. A polynomial of degree 5 has been fitted into the data. The 95% confidence interval from the fit is also represented. Finally, the 4-year data from Fermi-LAT is represented as the black dots and upper limits.

These are the results of the simulation for said values of the coronal radius, alpha and the turning angle, which are within reasonable expectation of the real values. However, it is also interesting to examine what the results of the model are for other values of R_c , α and θ_{\max} . This way, we can check whether there is a combination of these parameters which produces results that better fit the data from Fermi-LAT:

CHAPTER 4. RESULTS

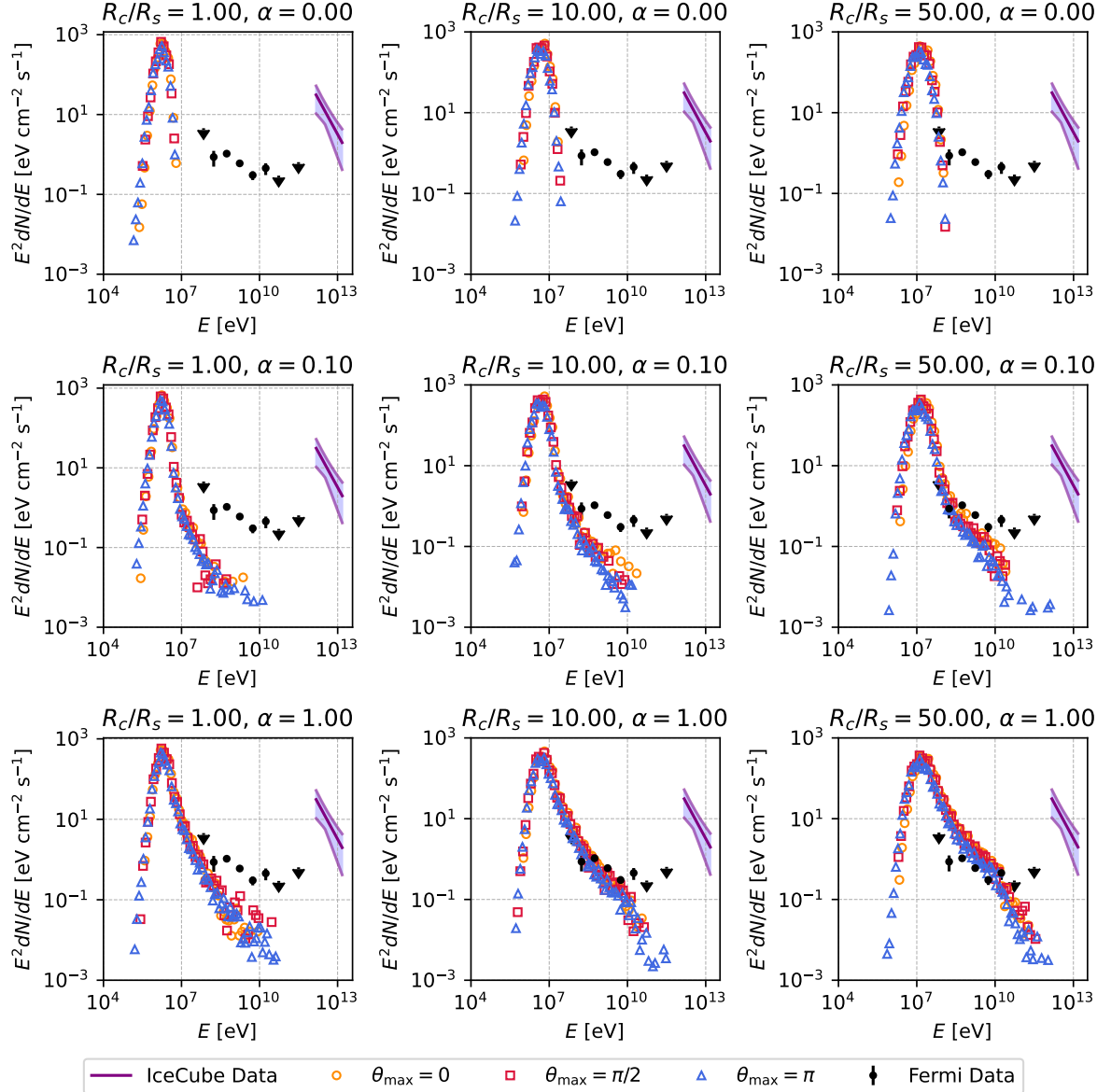


Figure 4.3: Spectral Energy Distribution of NGC 1068's AGN for different values of R_c/R_s , α and θ_{\max} . The purple line represents again the data from IceCube and our initial flux for the photons. The red, blue and yellow symbols represent the flux for different values of θ_{\max} . The 4-year data from Fermi-LAT is represented as the black dots and upper limits.

One interesting takeaway from this plot is that θ_{\max} has very little influence in the results. Beamed particles tend to have slightly higher energies due to the fact that they're prone to taking fewer steps when cascading. However, there is practically no difference between the particles executing a complete random walk and being beamed. This is due to the fact that the last step of the random walk is the one which matters the most: particles can take as many steps as they want, but if the last step's length is larger than

CHAPTER 4. RESULTS

the coronal radius, it will be the one which determines the final energy of the particle. Thus, the maximum turning angle of the particles has been neglected in the rest of the analysis, assuming it is equal to π (isotropic random walk).

These simulations are quite resource- and time-intensive. In order to find which parameters yield a better fit to the Fermi-LAT data, it is not practical to run the simulation for every possible combination of the parameters. Instead, we can use a machine learning algorithm to find the best fit. The idea is to use the simulated spectra as a training set for the algorithm, which will then be able to predict the shape of the spectrum given a certain combination of R_c and α ¹, effectively “interpolating” between the data:

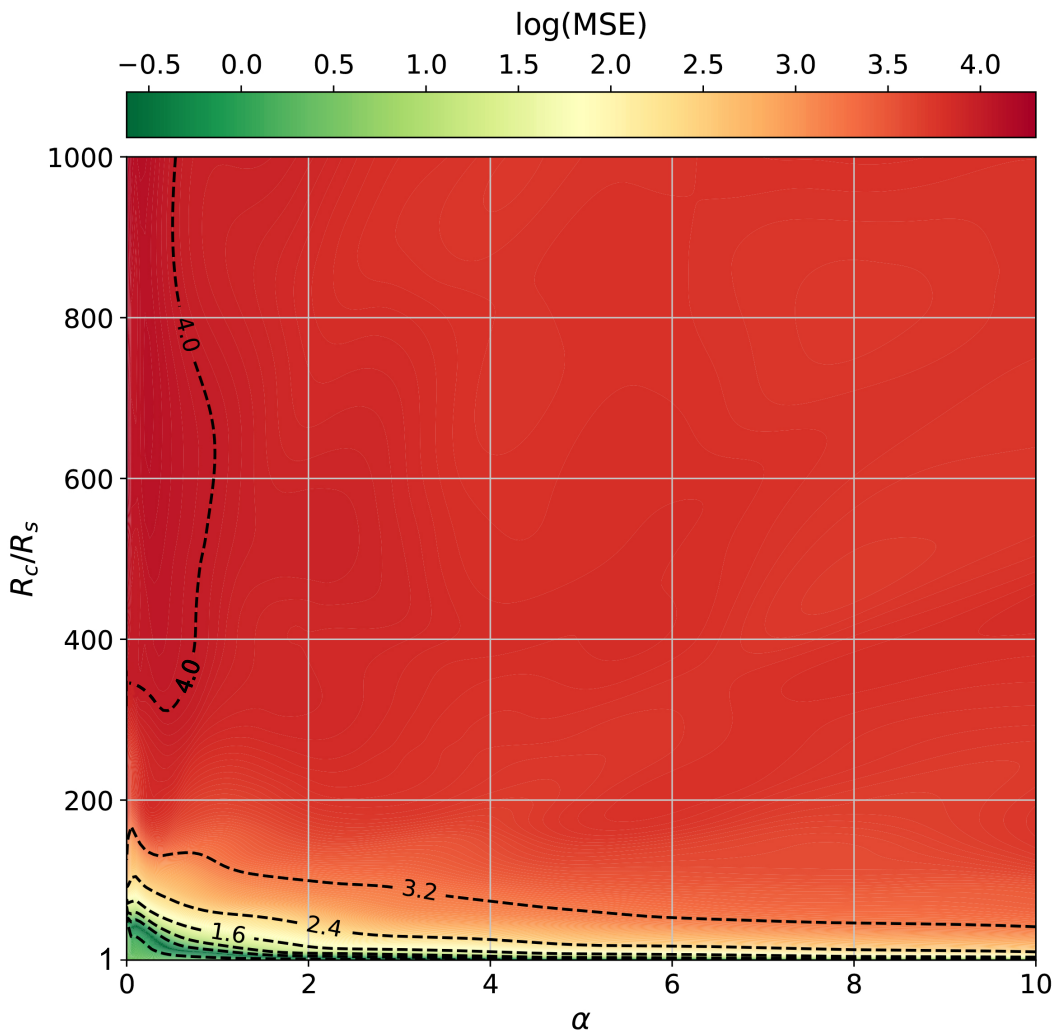


Figure 4.4: Goodness of fit as a function of α and R_c/R_s . The color scale represents the logarithm of the MSE (mean squared error) of the fit. In order to reduce noise from the neural network, the MSE has been averaged over 20 different runs.

¹Since the maximum turning angle’s effect has been shown to be negligible, I will simply assume the spectrum depends on said two parameters

CHAPTER 4. RESULTS

Figure 4.4 shows the goodness of fit for a large range of values of R_c . It can be seen that the MSE is very high regardless of α for R_c/R_s values above 100. The most interesting part of the plot is thus the region $R_c/R_s \in [1, 60]$. Plotting said region in more detail, we can get a better idea of the shape of the MSE as a function of the parameters:

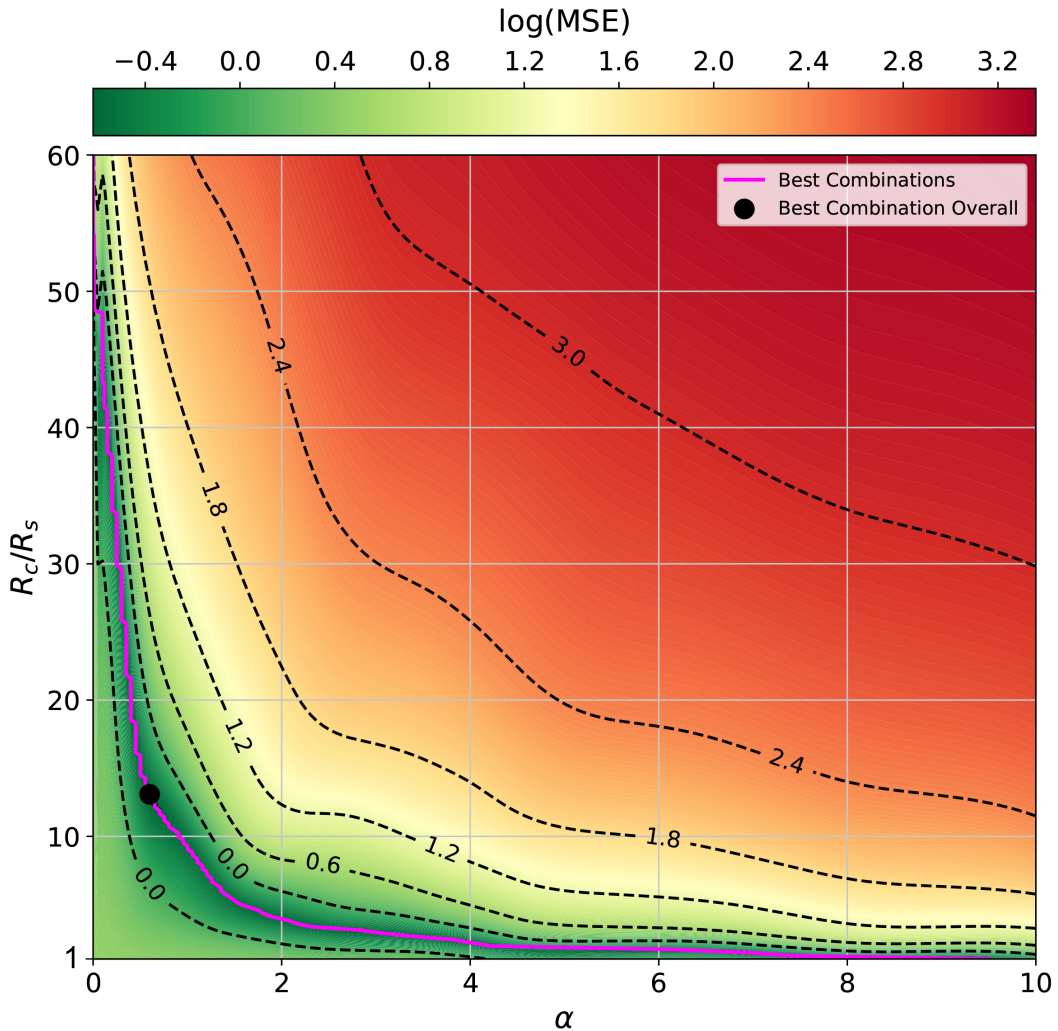


Figure 4.5: Goodness of fit as a function of α and R_c/R_s . The color scale represents the logarithm of the MSE of the fit. In order to reduce noise from the neural network even further, the MSE has been averaged over 30 different runs. Plotted are the best fits for each value of α , as well as the best combination of parameters overall.

There is a very clear trade-off between the two quantities: either the corona is very small and the particles start towards its edge, or the corona is large, but the particles begin their cascades very close to the center. The best fit for the whole range of α is located at $R_c/R_s \approx 13$, $\alpha \approx 0.6$. This is consistent with the values estimated earlier for the coronal radius of NGC 1068. One can also see that the MSE starts to irreversibly

CHAPTER 4. RESULTS

increase for values of R_c/R_s above 50, thus indicating that the coronal radius must not be larger than said value.

Now, all the different combinations of R_c and α can be sorted by their MSE, and then simulated, to check whether the neural network is able to predict the shape of the spectrum correctly. The following plot shows the SED for the best fit, as well as the 1000th, 3500th, 5000th up until the worst fit found by the algorithm:

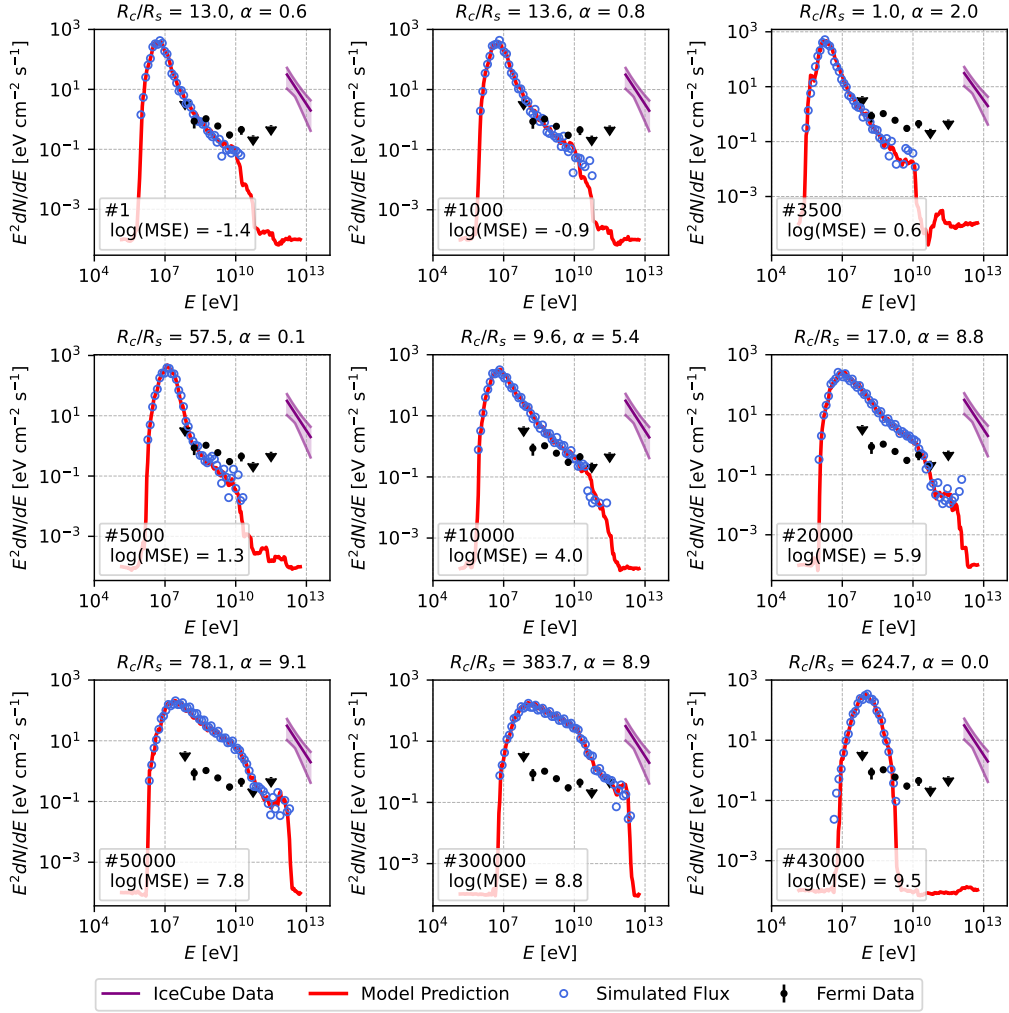


Figure 4.6: Spectral Energy Distribution of NGC1068's AGN for the best fit, as well as 1000th, 3500th, 5000th, up until the 430 000th. The purple line represents the data from IceCube (and our initial flux for the photons). The red line is the prediction from the neural network. Finally, the blue symbols represent the simulated flux. The 4-year data from Fermi-LAT is plotted as the black dots and upper limits. The legend shows the logarithm of the MSE of the fit, as well as the ordering of the simulations.

It is important to note that the MSE is not always a good measure of the goodness of fit. The prediction from the neural network has a noticeable “tail” at the end of the spectrum, which is not present in the simulated data. This is caused by the addition of

CHAPTER 4. RESULTS

synthetic data to the training set, in order to get the algorithm to train more accurately. This has the effect of creating artificial values in the prediction, which are not present in the simulated data. The result is that, for cases when α is very small, although the MSE is generally very high, it should be even higher. Take for example the 430 000th simulation. The MSE's logarithm has a value of ~ 10 , however, no data is actually present in the tail of the spectrum. This means that the flux for that part of the spectrum would be zero, and thus, the MSE would tend towards infinity.

Finally, another way of checking which parameters yield the best fit is to check the frequency of the different combinations of R_c and α whose MSE is below a certain threshold. The following plots show the frequency of the different combinations of R_c and α whose MSE is below 0.3 and 1:

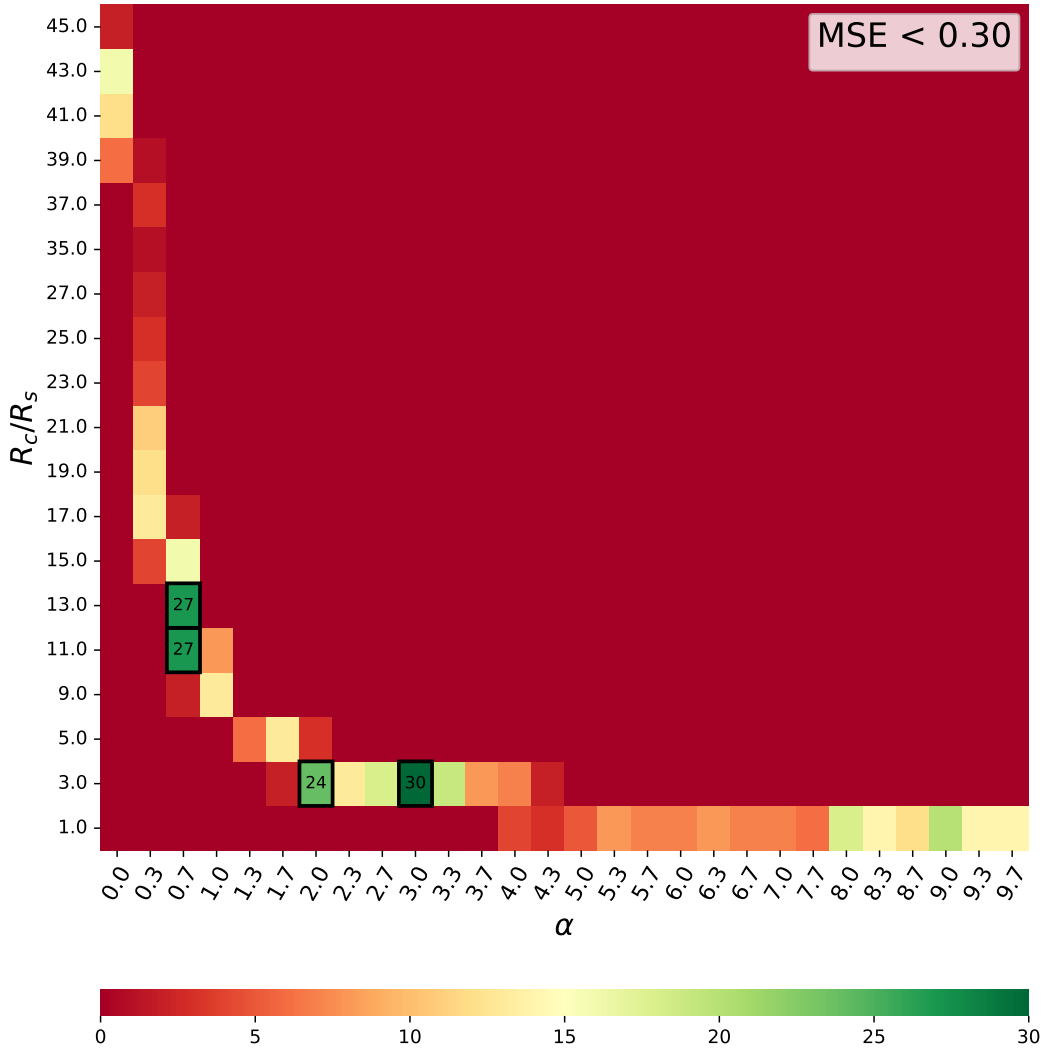


Figure 4.7: Heatmap of the frequency of the different combinations of α and R_c/R_s whose MSE doesn't exceed 0.3. Boxed in black are the top four combinations whose frequency is the highest.

CHAPTER 4. RESULTS

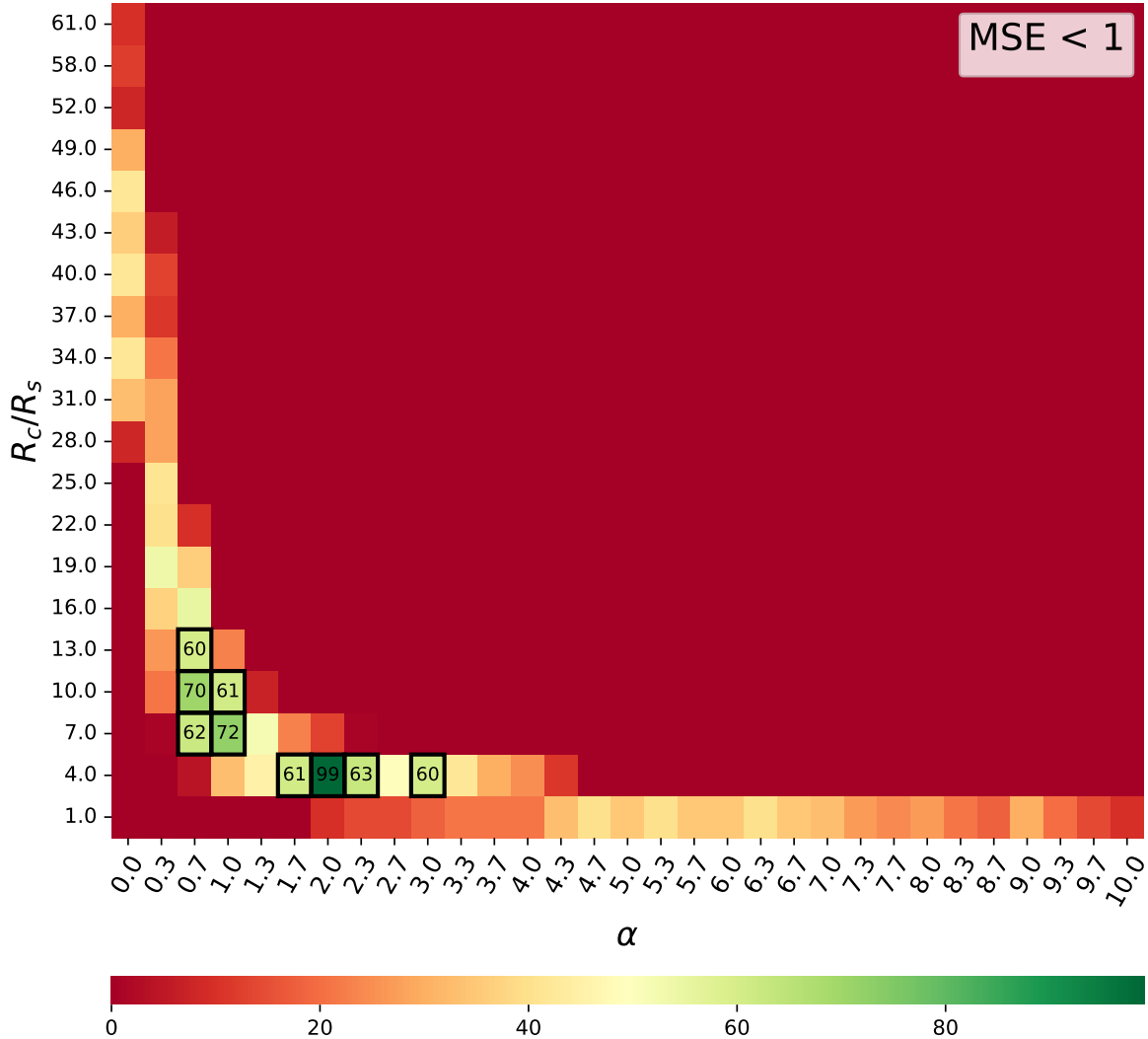


Figure 4.8: Heatmap of the frequency of the different combinations of α and R_c/R_s whose MSE doesn't exceed 1. Boxed in black are the top nine combinations whose frequency is the highest.

There are two main hotspots in these heatmaps: one at ($R_c/R_s \sim 10$, $\alpha \sim 0.8$), and another one at ($R_c/R_s \sim 3$, $\alpha \sim 2.3$). The first one is the same as the one found in the contour plots, while the second one is a bit more surprising. A coronal radius of $R_c/R_s \sim 3$ is very small, and would imply that the particles are starting very close to the center of the AGN. This is not consistent with the values found in the literature, which estimate the coronal radius to be at least $R_c/R_s \sim 10$. This suggests that the second hotspot might be an artifact of the model, or that the parameters are not well constrained in this region.

CHAPTER 4. RESULTS

4.1 Discussion

The results presented in this chapter offer valuable insight into the potential conditions we could find in the AGN of NGC 1068, which have been inferred by comparing the simulated cascaded particle flux with data obtained from missions such as Fermi-LAT. While simple, the random walk model is capable of capturing the essential nature of the phenomena at hand, as well as the resulting exponential energy loss per collision, as illustrated in Figure 4.1.

Comparing the simulated Spectral Energy Distributions (SEDs) with data from Ice-Cube and Fermi-LAT (Figures 4.2, 4.3 and 4.6) reveals the model's capability to reproduce the general trend of the observed gamma-ray flux at lower energies. An interesting result derived from the simulations is that of the low influence of the maximum turning angle, θ_{\max} , which likely stems from the dominant influence of the final interaction step's length on the particle's escape energy. This observation justified neglecting θ_{\max} in the subsequent, more computationally intensive parameter space exploration, simplifying the problem to the connection between the coronal radius (R_c) and the initial distribution parameter (α).

Given the computational demands of running full simulations for numerous parameter combinations, the machine learning approach proved essential. The contour plots derived from the neural network predictions (Figures 4.4 and, more importantly, 4.5) clearly delineate the valid parameter space. A distinct trade-off emerges between R_c and α : a smaller, more compact corona requires particles to start nearer the edge (higher α) to match the observed spectrum, whereas a larger corona demands particles starting closer to the central source (lower α) to undergo sufficient interactions. The region minimizing the Mean Squared Error (MSE) centers around $R_c/R_s \approx 13$ and $\alpha \approx 0.6$, which fits reasonably well with independent estimates for NGC1068's coronal radius found in the literature (Eichmann et al., 2022).

The frequency analysis presented in Figures 4.7 and 4.8 further reinforces these findings. By mapping the density of parameter combinations yielding low MSE values, these heatmaps highlight the same preferred region identified in the contour plots, confirming the robustness of the best-fit parameters within the model's framework.

However, certain limitations must be acknowledged. The comparison between the neural network predictions and direct simulations (Figure 4.6) revealed discrepancies, particularly the artificial "tail" in the predicted spectra at low energies for high MSE fits. This artifact, arising from the use of synthetic data during training, shows that the MSE, while a useful metric, may not perfectly capture the goodness-of-fit for different parameters, especially in regimes where the model performs poorly (e.g., very low α). The true MSE in such cases might be significantly higher than calculated due to the sharp cutoff in simulated flux versus the predicted tail. It must also be acknowledged that although the simulations allow for the coronal radius to be just as small as the Schwarzschild radius, this is not a realistic assumption. The coronal radius ought to be larger than the Black Hole's event horizon. Otherwise, the particles wouldn't be able to escape the AGN at all.

Chapter 5

Outlook

This work has explored the discrepancy between the observed high-energy neutrino flux and the suppressed gamma-ray flux from NGC 1068 by developing a model centered on electromagnetic cascading within the AGN’s corona. Using a combination of random walk simulations and machine learning techniques, it was demonstrated that such cascades can indeed reproduce the observed gamma-ray attenuation while constraining the physical parameters of the corona, notably finding a preferred region around $R_c/R_s \approx 13$ and $\alpha \approx 0.6$. Furthermore, the model predicts a characteristic reprocessing signature: an excess of lower-energy gamma rays in the MeV range.

While the model successfully captures key aspects of the phenomenon, several simplifications and approximations were made, opening avenues for future refinement and investigation.

5.1 Model Refinements

The current implementation of the random walk includes several approximations, which could be addressed in more refined models:

- **Scattering and Energy Loss:** The assumption of isotropic scattering and a fixed energy loss fraction (approximately 50%) per interaction simplifies the complex physics of pair production and subsequent particle interactions. Implementing more realistic, energy-dependent differential cross-sections for scattering and a more detailed treatment of energy partitioning in pair production and inverse Compton scattering by the created pairs would enhance the model’s fidelity.
- **Cascade Development:** The current approach approximates the cascade by multiplying the escaping particle count based on the number of collisions, rather than explicitly tracking all secondary electrons and positrons, which subsequently perform cascades of their own. A full Monte Carlo simulation tracking all generations of particles, including their potential energy losses via synchrotron radiation and inverse Compton scattering within the corona’s magnetic and photon fields, would provide a more accurate picture of the cascade development and the resulting energy spectrum.
- **Magnetic Field and Geometry:** The influence of the magnetic fields inside the AGN is currently not accounted for in the model. Incorporating magnetic field

CHAPTER 5. OUTLOOK

geometries could affect particle trajectories and introduce synchrotron losses for the electron-positron pairs, potentially altering the cascade dynamics and escape probabilities. Similarly, assuming a simple, homogeneous spherical corona with an isotropic distribution of background radiation might be an oversimplification.

- **Background Photon Field:** The model relies on a static background photon field derived from previous studies (as shown in Figure 3.1), with the caveat of potential circular reasoning noted in Chapter 3. A self-consistent approach, where the cascaded photon spectrum iteratively informs the background field for subsequent calculations, could capture feedback effects (although this would significantly increase computational complexity).

5.2 Computational Enhancements

The reliance on a neural network to explore the parameter space, while necessary due to computational costs, introduced certain artifacts, such as the low-energy "tail" in predictions for high-MSE fits (Figure 4.6). Future work could explore:

- **Advanced Machine Learning:** Utilizing different network architectures, loss functions beyond MSE that might better capture spectral shape, or alternative machine learning techniques could potentially mitigate prediction artifacts and improve the accuracy of parameter inference. Training strategies could also be refined to reduce reliance on synthetic data.
- **Computational Efficiency:** Even though a good portion of the time was spent optimizing the simulation code, there are lots of ways in which this section of the work could be improved. Implementing GPU acceleration, in order to simulate more particles in parallel, could allow for running more detailed simulations (e.g., full secondary tracking) over a wider range of parameters, reducing the dependence on machine learning interpolation.

5.3 Future Observational Tests

The model makes specific predictions that are potentially testable with current and future observational facilities:

- **The MeV Excess:** The most distinct prediction is the pile-up of reprocessed photons in the 10^6 – 10^8 eV (1-100 MeV) range. While challenging to observe due to high backgrounds and instrumental limitations, future proposed MeV gamma-ray telescopes (such as concepts like AMEGO-X (Caputo et al., 2022) or e-ASTROGAM (De Angelis et al., 2017)) could potentially detect or constrain this signature, providing strong validation (or refutation) of the cascade scenario. Continued analysis of Fermi-LAT data in this range might also yield constraints.

CHAPTER 5. OUTLOOK

- **Coronal Constraints:** The derived coronal size ($R_c/R_s \approx 13$) could be indirectly tested. High-resolution X-ray spectroscopy (e.g., with XRISM or future missions like Athena) might probe the conditions and extent of the hot coronal gas through spectral line analysis or reverberation mapping. Similarly, advancements in millimeter VLBI could potentially resolve structures on scales approaching the predicted coronal size for nearby AGN like NGC 1068.
- **Variability Studies:** Correlated variability studies between X-ray emission (probing the corona) and gamma-ray/neutrino emission could provide insights into the location and dynamics of the particle acceleration and interaction regions, further constraining the model’s parameters.
- **Application to Other Sources:** Applying this modeling framework to other AGNs detected or suspected as neutrino sources (e.g., TXS 0506+056 (Mark Aartsen et al., 2018)) would test the generality of the model and the derived relationships between coronal properties and multi-messenger emission.

In summary, while this work provides a viable (although simplified) framework for understanding the gamma-ray suppression in NGC 1068 through electromagnetic cascading, further theoretical refinements and observational campaigns, particularly in the MeV gamma-ray band, could shed more light onto how the complex environment of AGNs actually operates.

References

- Aartsen, M.G. et al. (Mar. 2017). “The IceCube Neutrino Observatory: instrumentation and online systems”. In: *Journal of Instrumentation* 12.03, P03012–P03012. ISSN: 1748-0221. DOI: 10.1088/1748-0221/12/03/p03012. URL: <http://dx.doi.org/10.1088/1748-0221/12/03/P03012>.
- Aartsen, Mark et al. (July 2018). “Neutrino emission from the direction of the blazar TXS 0506+056 prior to the IceCube-170922A alert”. In: *Science* 361.6398, pp. 147–151. ISSN: 1095-9203. DOI: 10.1126/science.aat2890. URL: <http://dx.doi.org/10.1126/science.aat2890>.
- Abbasi, R. et al. (2022). “Evidence for neutrino emission from the nearby active galaxy NGC 1068”. In: *Science* 378.6619, pp. 538–543. DOI: 10.1126/science.abg3395. eprint: <https://www.science.org/doi/pdf/10.1126/science.abg3395>. URL: <https://www.science.org/doi/abs/10.1126/science.abg3395>.
- Abdollahi, S. et al. (June 2022). “Incremental Fermi Large Area Telescope Fourth Source Catalog”. In: *The Astrophysical Journal Supplement Series* 260.2, p. 53. ISSN: 1538-4365. DOI: 10.3847/1538-4365/ac6751. URL: <http://dx.doi.org/10.3847/1538-4365/ac6751>.
- Berezinsky, V. and O. Kalashev (July 2016). “High-energy electromagnetic cascades in extragalactic space: Physics and features”. In: *Physical Review D* 94.2. ISSN: 2470-0029. DOI: 10.1103/physrevd.94.023007. URL: <http://dx.doi.org/10.1103/PhysRevD.94.023007>.
- Blanco, Carlos et al. (2023). *On the Neutrino and Gamma-Ray Emission from NGC 1068*. arXiv: 2307.03259 [astro-ph.HE]. URL: <https://arxiv.org/abs/2307.03259>.
- Caputo, Regina et al. (Oct. 2022). “All-sky Medium Energy Gamma-ray Observatory eXplorer mission concept”. In: *Journal of Astronomical Telescopes, Instruments, and Systems* 8.04. ISSN: 2329-4124. DOI: 10.1117/1.jatis.8.4.044003. URL: <http://dx.doi.org/10.1117/1.JATIS.8.4.044003>.
- Chiu, Hong-Yee (May 1964). “Gravitational collapse”. In: *Physics Today* 17.5, pp. 21–34. ISSN: 0031-9228. DOI: 10.1063/1.3051610. eprint: <https://pubs.aip.org/physicstoday/article-pdf/17/5/21/8261856/21\1\online.pdf>. URL: <https://doi.org/10.1063/1.3051610>.
- Collinson, James S. et al. (Oct. 2016). “Reaching the peak of the quasar spectral energy distribution – II. Exploring the accretion disk, dusty torus and host galaxy”. In: *Monthly Notices of the Royal Astronomical Society* 465.1, pp. 358–382. ISSN: 1365-2966. DOI: 10.1093/mnras/stw2666. URL: <http://dx.doi.org/10.1093/mnras/stw2666>.

REFERENCES

- De Angelis, A. et al. (June 2017). “The e-ASTROGAM mission: Exploring the extreme Universe with gamma rays in the MeV – GeV range”. In: *Experimental Astronomy* 44.1, pp. 25–82. ISSN: 1572-9508. DOI: 10.1007/s10686-017-9533-6. URL: <http://dx.doi.org/10.1007/s10686-017-9533-6>.
- Eichmann, Björn et al. (Nov. 2022). “Solving the Multimessenger Puzzle of the AGN-starburst Composite Galaxy NGC 1068”. In: *The Astrophysical Journal* 939.1, p. 43. ISSN: 1538-4357. DOI: 10.3847/1538-4357/ac9588. URL: <http://dx.doi.org/10.3847/1538-4357/ac9588>.
- Ghisellini, Gabriele (2013). *Radiative Processes in High Energy Astrophysics*. Springer International Publishing. Chap. 8. ISBN: 9783319006123. DOI: 10.1007/978-3-319-00612-3. URL: <http://dx.doi.org/10.1007/978-3-319-00612-3>.
- Kachelrieß, M., S. Ostapchenko, and R. Tomàs (Apr. 2012). “ELMAG: A Monte Carlo simulation of electromagnetic cascades on the extragalactic background light and in magnetic fields”. In: *Computer Physics Communications* 183.4, pp. 1036–1043. ISSN: 0010-4655. DOI: 10.1016/j.cpc.2011.12.025. URL: <http://dx.doi.org/10.1016/j.cpc.2011.12.025>.
- Kowalski, Marek and for the IceCube Collaboration (Sept. 2017). “Neutrino astronomy with IceCube and beyond”. In: *Journal of Physics: Conference Series* 888.1, p. 012007. DOI: 10.1088/1742-6596/888/1/012007. URL: <https://dx.doi.org/10.1088/1742-6596/888/1/012007>.
- Mücke, A. et al. (1999). “Photohadronic Processes in Astrophysical Environments”. In: *Publications of the Astronomical Society of Australia* 16.2, pp. 160–166. ISSN: 1448-6083. DOI: 10.1071/as99160. URL: <http://dx.doi.org/10.1071/AS99160>.
- Padovani, P. et al. (2024). *High-energy neutrinos from the vicinity of the supermassive black hole in NGC 1068*. arXiv: 2405.20146 [astro-ph.HE]. URL: <https://arxiv.org/abs/2405.20146>.
- Skrutskie, M. F. et al. (Feb. 2006). “The Two Micron All Sky Survey (2MASS)”. In: *The Astronomical Journal* 131.2. DOI: 10.1086/498708. URL: <https://dx.doi.org/10.1086/498708>.
- Wang, Jian-Min et al. (July 2020). “Dynamical evidence from the sub-parsec counter-rotating disk for a close binary of supermassive black holes in NGC 1068”. In: *Monthly Notices of the Royal Astronomical Society* 497.1, pp. 1020–1028. ISSN: 0035-8711. DOI: 10.1093/mnras/staa1985. eprint: <https://academic.oup.com/mnras/article-pdf/497/1/1020/33538385/staa1985.pdf>. URL: <https://doi.org/10.1093/mnras/staa1985>.

A - GitHub repository

The MATLAB code utilized in this project can be found in the following repository, as well as the LaTeX source code for this thesis and some additional resources, such as Manim animations:

GitHub repository link

- <https://github.com/pauverblom/TFG>